Journal of Power Sources 201 (2012) 26–36

Contents lists available at SciVerse ScienceDirect

Journal of Power Sources

journal homepage: www.elsevier.com/locate/jpowsour

Synthesis and performance of A-site deficient lanthanum-doped strontium titanate by nanoparticle based spray pyrolysis

Dariusz Burnat[a,b,*], Andre Heel[c,3], Lorenz Holzer[a,1], Dariusz Kata[b,2], Jerzy Lis[b,2], Thomas Graule[a,1]

[a] Empa, Swiss Federal Laboratories for Materials Science and Technology, Laboratory for High Performance Ceramics, Ueberlandstrasse 129, CH-8600 Dübendorf, Switzerland
[b] AGH – University of Science and Technology, Faculty of Materials Science and Ceramics, Department for Technology of Ceramics and Refractories, Mickiewicza 30, 30-059 Cracov, Poland
[c] Empa, Swiss Federal Laboratories for Materials Science and Technology, Marketing and Technology Transfer, Ueberlanstrasse 129, CH-8600 Dübendorf, Switzerland

ARTICLE INFO

Article history:
Received 11 May 2011
Received in revised form 3 October 2011
Accepted 24 October 2011
Available online 30 October 2011

Keywords:
SOFC
Ceramic anodes
Strontium titanate
Redox
Spray pyrolysis
Nanoparticles

ABSTRACT

In this study A-site deficient lanthanum doped strontium titanate, which is considered as a promising, redox-stable candidate for full ceramic anodes in Solid Oxide Fuel Cells (SOFCs), was produced by nanoparticle-based spray pyrolysis. In this process cost-effective nitrate salts and titania nanoparticles are used as precursors. LST with a nominal composition of $La_{0.2}Sr_{0.7}TiO_3$ showed limited stability at temperatures higher than 1290 °C. It was observed that minor contents of secondary phases, which form at elevated temperatures, invoke a drastic loss of the electrical performance. Thermal stability is significantly increased by a slight enrichment of strontium. The phase pure A-site deficient LST shows remarkably higher electrical performance than similar stoichiometric counterparts. Reductive sintering results in a conductivity as high as 600 S cm^{-1} at 600 °C. Furthermore the A-site deficient LST shows a high redox-stability and fast redox-kinetics. With these properties LST is a suitable material for the fabrication of a new generation of Ni-free ceramic SOFC anodes. Secondary phases have a significant influence on the electrical conductivity and redox behaviour.

1. Introduction

State-of-the-art SOFC anodes consist of nickel cermets with yttrium-stabilized zirconia (YSZ) or with gadolinium doped ceria (GDC). However, besides the excellent electrochemical performance, the cermet anodes do suffer from coarsening of nickel grains and from volume changes during redox cycling, which leads to the disruption of the percolation of the electronically conductive phase [1–7]. Furthermore, the cermet anodes tend to form carbon filaments on the nickel surface from the hydrocarbon atmosphere, which reduce the catalytic activity. For future SOFC applications it is thus a major challenge to circumvent the degradation problems associated with the nickel cermet materials, which could be achieved by replacing the nickel by a redox-stable ceramic material with sufficient electrical and catalytic activities.

Currently particular attention is paid to lanthanum or yttrium doped strontium titanates, which provide excellent redox stability over a wide range of oxygen partial pressures (pO_2). One of the most interesting properties of lanthanum doped strontium titanates (LSTs) is a relatively high electronic conductivity and very good sulphur resistance [8–10]. It was shown that a LST-based cell can be operated without significant degradation with sulphur contents as high as 5000 ppm [11,12]. This sulphur content is several orders of magnitudes higher than what conventional state-of-the-art Ni-YSZ can withstand. Marina et al. performed an extensive research about thermal, electrical and electrochemical properties of stoichiometric lanthanum strontium titanates [13]. They reported reversible change of conductivity during reduction–oxidation tests for specimens sintered in air, which show acceptable conductivity values. Fu and Tietz were studying redox stability and performance of various co-doped titanates [14], but the fact that the nominal composition of $Sr_{0.41}La_{0.4}TiO_3$ cracked during reoxidation, might raise some doubts about the applicability of this LST composition. In contrast Savaniu and Irvine [15] have successfully applied A-site deficient LST as an anode material in well performing button cells. A-site deficient LSTs are perceived as interesting anode materials, since the deficiency can lead to increased conductivity values. In addition A-site deficient perovskite has a lower tendency to react with the zirconia electrolyte and to form secondary phases such as insulating $La_2Zr_2O_7/SrZrO_3$, as it is well known from several cathode materials containing lanthanum and strontium [16–21]. These promising results show that LST in general is an interesting material for the application in SOFC anodes. However, the cost efficient synthesis of

* Corresponding author at: AGH – University of Science and Technology, Faculty of Materials Science and Ceramics, Department for Technology of Ceramics and Refractories, Mickiewicza 30, 30-059 Cracov, Poland. Tel.: +48 012 617 5002; fax: +48 012 633 1593.
E-mail address: dburnat@gmail.com (D. Burnat).
[1] Tel.: +41 044 823 4844; fax: +41 044 823 4150.
[2] Tel.: +48 012 617 5002; fax: +48 012 633 1593.
[3] Tel.: +41 058 765 4199; fax: +41 058 765 4008.

0378-7753/$ – see front matter © 2011 Elsevier B.V. All rights reserved.
doi:10.1016/j.jpowsour.2011.10.088

Table 1
Summary of processing routes and properties of lanthanum doped strontium titanates from literature (SSR: solid state route, GNP: glycine-nitrate process, NSP: spray pyrolysis).

Chemical formula	Stoichiometry parameters	Processing route	Ref.
Stoichiometric			
$La_xSr_{1-x}TiO_3$	0.1–0.4	GNP	[13]
	0.1–0.4	SSR	[8]
	0.001–0.05	SSR	[20,21]
	0.2–0.5	SSR	[22]
	0.33	SSR	[23]
A-site deficient			
$Sr_{1-3x/2}La_xTiO_{3-\delta}$	0.4–0.6	SSR	[24]
$Sr_{1-3x/2}La_xTiO_{3-\delta}$	0.2	SSR	[15]
$Sr_{1-3x/2}La_xTiO_{3-\delta}$	0.2	NSP	This work

phase pure, homogenous and fine grain LST powders is a challenging task, which requires careful evaluation of a reliable synthesis route and of suitable stoichiometries.

1.1. Synthesis routes of LST

Different production routes for LST powders reported in literature are summarized in Table 1. Several methodologies for the preparation of LST ceramic anodes have been tested. Overall, the solid state route (SSR) represents the synthesis method which is most commonly applied due to its simplicity. However, the main drawbacks are relatively long calcination periods at relatively high temperatures and the tendency to form chemical heterogeneities. Additionally unreacted precursors and very intensive milling that has to be performed after the synthesis may introduce a significant level of impurity. Many of the problems are related to the high temperatures, which results in heterogeneous compositions with excessive grain growth. These high temperatures in combination with relatively long preparation time are required for the processing of relatively coarse raw materials. In order to increase the material's purity and therefore eliminate secondary phases a step-wise calcination–regrinding–calcination procedure is usually carried out. This procedure is not suitable for the production of larger quantities of high purity materials that are necessary for fuel cell development and fabrication. Thereby a particular problem may arise from free lanthanum and titania compounds, which are not incorporated into the LST crystal lattice. These free compounds may easily react with electrolyte material, thus creating insulating reaction products.

In order to circumvent the problems associated with the conventional synthesis route, the nanoparticle based spray pyrolysis (NSP process) is evaluated in this study as an alternative synthesis route for efficient production of homogenous, single phase and fine grained LST powders. In addition to macroscopic characteristics (phase purity, grain size, etc.) electrical conductivity, electrochemical activity and redox stability are strongly dependent on microscopic aspects such as defect chemistry and charge compensation mechanism. Therefore some basic principles of defect chemistry are discussed subsequently specifically for the LST-system.

1.2. The defect chemistry and compensation mechanism donor of doped strontium titanate

$SrTiO_3$ (ST) is a cubic perovskite (ABO_3) with insulating properties in oxidizing atmosphere. Under reducing conditions it becomes conductive, due to the oxygen removal from the crystal lattice:

$$2Ti_{Ti}^{x} + O_O^x \overset{SrTiO_3}{\longleftrightarrow} 2Ti'_{Ti} + V_O^{\bullet\bullet} + \frac{1}{2}O_{2(g)} \quad (1)$$

or

$$O_O^x \leftrightarrow 2e' + V_O^{\bullet\bullet} + \frac{1}{2}O_{2(g)} \quad (2)$$

The reduction of titanium is the driving force that introduces electrons to the Ti-3d orbital. Therefore, the electronic properties are directly related to the concentration of trivalent titanium [22,23]. However, the formation of oxygen vacancies $SrTiO_3$ is limited which is the reason why polycrystalline strontium titanate only shows moderate to low conductivities [24]. The introduction of donor dopants (e.g. La, Y, Gd) enhances the electronic conductivity under reducing conditions [25,26]. The stability and the electrical properties are strongly related to the crystal structure at different dopant contents and reduction states as a function of oxygen partial pressure. Therefore the defect chemistry of stoichiometry and non-stoichiometry is discussed separately.

1.2.1. Stoichiometric LST

The changes from a $SrTiO_3$ to a stoichiometric $LaSrTiO_3$ can be described as a 'one-to-one substitution' of Sr by La, whereby the A-site remains fully occupied and the A-site to B-site ratio remains 1. For a fully reduced material the concentration of trivalent titania should be equal to the doping level of La:

$$[La_{Sr}^{\bullet}] = [Ti'_{Ti}] \quad (3)$$

In oxidizing atmosphere trivalent titanium is not likely to appear. In order to maintain charge neutrality a different compensation mechanism is introduced. Thereby the accommodation of excess oxygen leads to the creation of oxygen-rich defect regions and structure rearrangement [27–30]. The way in which the oxygen is accommodated strongly depends on the dopant concentration. For highly doped $LaSrTiO_3$ the crystallographic shear structures $La_2Ti_2O_7$–$SrTiO_3$ exist, while at lower La doping levels randomly distributed linear defects and point defects are created [29], which influence the redox stability and conductivity [31]. Thus, in order to maintain charge neutrality, excess oxygen is introduced and can be expressed as interstitially and randomly localized defects:

$$La_2O_3 + 2Sr_{Sr}^{x} \leftrightarrow 2SrO + 2La_{Sr}^{\bullet} + O_i'' \quad (4)$$

with the corresponding charge neutrality condition:

$$[La_{Sr}^{\bullet}] = 2\left[O_i''\right] \quad (5)$$

Consequently, stoichiometric LST contains high amounts of interstitial oxygen, if sintered at high pO_2 pressures, which is usually described with the term '$+\delta$' (the stoichiometric compositions should be thus written as: $La_xSr_{1-x}TiO_{3+\delta}$). When exposed to a low oxygen partial pressure, the oxygen is removed from the LST crystal lattice. The free electrons associated with the oxygen removal will recombine with Ti, what leads to a decrease of the B-site valence from Ti^{4+} to Ti^{3+}:

$$2e' + 2Ti_{Ti}^{x} \leftrightarrow 2Ti'_{Ti} \quad (6)$$

The existence of trivalent Ti leads to n-type semiconducting behaviour, which is also called 'reduction type semiconduction'. The underlying charge transport mechanism is assumed to be of a so-called 'hopping-type', whereby electrons are moving from a Ti^{3+} to the neighbouring Ti^{4+}. It is evident the degree of Ti-reduction is of major importance in order to reach a high electrical conductivity.

1.2.2. Understoichiometric LST

It is known from literature that non-stoichiometric LST compositions exist within a certain range of compositions [32–34]. The non-stoichiometric compositions described by the general formula of $La_xSr_{1-0.5x}TiO_3$ have a variable A-to-B ratio, which depends on the dopant concentration (^{x}). Upon doping the additional charge from the La^{3+} can be compensated by the formation of Sr-vacancies

on the A-site. In this way no oxygen uptake is necessary to compensate for the additional charge.

$$La_2O_3 + 2Sr_{Sr}^{x} \leftrightarrow 2SrO + 2La_{Sr}^{\bullet} + V_{Sr}'' + \frac{1}{2}O_{2(g)} \quad (7)$$

The corresponding charge neutrality condition is then written as follows:

$$[La_{Sr}^{\bullet}] = 2\left[V_{Sr}''\right] \quad (8)$$

Thereby, the amount of Sr-vacancies in the A-site deficient perovskites is defined as $x/2$, whereby x = La. The La-rich end member has a maximum dopant-content with $x = 0.66$ (i.e. $La_{0.66}TiO_3$) and a vacancy concentration of 33% on the A-site. Upon reduction of A-site deficient LST the low pO_2 leads to the formation of oxygen vacancies in a similar way as described for stoichiometric LST in Eqs. (1) and (2). This, in turn, results in the electronic compensation of the lanthanum charge by the change of the valence state on the B-site (Eq. (6)), which introduces n-type conductivity.

At this stage however it is not clear to what extent the above mentioned planar or linear defects (in stoichiometric LST) and of Sr-vacancies (in deficient LST) may influence the macroscopic materials properties. It is however clear that the different defect structures will lead to significantly different properties, such as phase stability, redox behaviour and conductivity. So far, the relationship of the material properties with the variable defect structures associated with different degrees of A-site doping of deficient lanthanum doped strontium titanates has not been investigated in a systematic way and so far no study was dealing with the suitability of those A-site deficient compounds.

In this study we aim to prepare larger quantities of phase pure LST-powder (i.e. between 500 and 2000 g). The properties of these titanate powders may be strongly dependent on the processing history and on the preparation conditions of the material. Therefore, in this work the goal is to investigate the properties of $La_{0.2}Sr_{0.7}TiO_3$ produced by the nanoparticle based spray pyrolysis (NSP). Particular attention is given to the phase purity of the powders, the thermal stability and to the corresponding properties, which are linked with specific defect chemistry of deficient lanthanum strontium titanate.

2. Experimental

2.1. Powder preparation by nanoparticle based spray pyrolysis (NSP) and by solid state synthesis route (SSR)

It is the intention of the present study to circumvent the problems related to LST synthesis with solid state techniques, which are summarized in Section 1, by applying alternative production techniques. For this purpose, spray pyrolysis (SP) fulfils most requirements for a cost effective production of LST powders with varying compositions and a wide range of particle size distributions [35–38]. However, the selection of Ti-precursors for spray pyrolysis is strongly limited with respect to suitable chemical components and cost-effectiveness. Moderately expensive precursors are unsuitable due to hydrolysis and precipitation in aqueous solutions, while organic solvents generally have too low solubility of Ti. Alternatively, the selection of titania nanoparticles as a precursor is particularly attractive due to its relatively low-cost and short diffusion pathways due to the small size of primary particles (as discussed below).

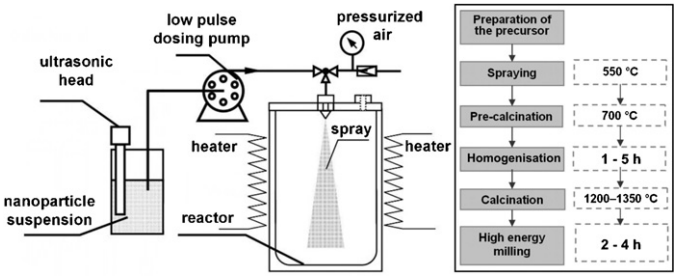

Fig. 1. Schematic illustration of the equipment (left) for nanoparticle based spray pyrolysis (NSP) with a diagram of the corresponding work flow for the LST production (right).

The starting solution was made by mixing a certain amount of combustive compound—gelatine in deionised water. Stoichiometric amounts of lanthanum and strontium salts were then added to a previously prepared gelatine solution. The homogenisation was carried out within a 12 h period. The precursor reagents used for the synthesis of LST with NSP are summarized in Table 2.

During spray pyrolysis, an aerosol spray of the precursor solution is introduced into a reactor or furnace where the droplets are thermally decomposed to form oxide particles. In contrast to the conventional spray pyrolysis, which is typically a single step process, the chamber-wise route requires post treatment by means of homogenisation and calcination at specified temperatures. In this study chamber-wise pyrolysis was performed in a pot furnace (Kittec CB65). The atomisation of the precursor suspension was carried out at 550 °C, followed by the decomposition of nitrate residues performed at 700 °C for 4 h. A peristaltic pump (Watson-Marlow 505S/505L head) was employed in order to assure high dosing accuracy and pulse free dosing to maintain a constant droplet size distribution (see Fig. 1).

For comparison also conventional LST production was performed. The solid state route synthesis was carried out from the same reagents which are listed in Table 2. The reagents were mixed according to the stoichiometric proportions of the LST-composition. Suspended in isopropanol reagents were homogenised in a planetary ball mill at 350 rpm for 10 h (1l vessel, ZrO_2 milling balls 1–10 mm). The calcination was carried out at 1200 °C, 1300 °C and 1400 °C.

2.2. Material characterisation

The crystal structure of calcined powders was analysed by X-ray diffraction (PANalytycal X'pert Pro MPD, Netherlands equipped with a Johanson monochromator) with Cu-Kα (λ = 1.5405 Å). The measurements were carried out within a 2Θ range of 5–80°. The specific surface area (SSA) of powders that were pre-dried at 180 °C for 2 h was determined by a five-point nitrogen adsorption isotherm at −196 °C (Coulter electronics USA, SA 3100).

Table 2
Raw materials and main expected gelatine-derivatives used as precursors for the LST production with NSP and SSP.

Systematic name	Chemical formula	Mol. mass (g mol^{-1})	Purity (%)	Function	Supplier
Strontium nitrate	$Sr(NO_3)_2$	211.63	Puriss >99	Reagent	Sigma–Aldrich
Lanthanum nitrate hexahydrate	$La(NO_3)_3{\cdot}6H_2O$	433.03	Puriss 99.99	Reagent	Auer Remy
Titania/titanium dioxide	TiO_2 (anatase/rutile = 76:24)	79.87	Puriss 99.99	Nanopowder reagent	Evonik Industries
Titanium dioxide	TiO_2 rutile	79.87	99.5	Reagent	Cerac
Strontium carbonate	$SrCO_3$	147.63	99.9	Reagent	Sigma–Aldrich
Lanthanum oxide	La_2O_3	325.81	99.99	Reagent	Auer Remy

The conductivity measurements were made using the four point DC technique (Keithley 2750). For this purpose calcined and milled powders were uni-axially pressed at 320 MPa and sintered at temperatures between 1240 °C and 1450 °C. In order to ensure good electric contacts between the samples and the contact wires the specimens were brushed with platinum paste (Metalor), dried at 120 °C for 1 h and fired afterwards at 1000 °C for 1 h. Specimens were then wrapped up by Pt wires (noble metals, Pt 99.99%, d = 0.3 mm) and connected to the measuring terminal. The conductivity measurements were carried out in both oxidizing (N_2/O_2 artificial air, 99.9995) and reducing atmospheres. A mixture of forming gas was created with previously calibrated mass flow controllers (MFC) (Vogtlin instruments, GSC-A, Get-Ready). Forming gas of 5% hydrogen (H_2, 99.995%, PanGas, Switzerland) in nitrogen (N_2, 99.995, PanGas, Switzerland) was used during the whole investigation. The oxygen partial pressure was monitored with a lambda sensor (Cambridge Rapidox 2100).

The microstructure of cross sections was investigated with scanning electron microscopy (Tescan Vega 5130-SB). Samples were embedded in resin, cured and polished. The particle morphology of produced powders was evaluated with a FEG-SEM (FEI, Nova NanoSEM230) that is equipped with a STEM-detector. For this purpose powders were dispersed in alcohol with ultrasonic treatment, from which single drops were added onto a copper TEM grid and then dried.

Reoxidation of the LST leads to an increase of weight, which was measured by thermo-gravimetric analysis (Netzsch STA 409). The specimen was sintered at 1430 °C and cooled down to room temperature in flowing forming gas (5%) and then grinded to a fine powder. The procedure was calibrated by a separate measurement of the empty supporting crucible. Subsequently, the specimen was heated up in forming gas to the temperature of 980 °C, flushed with argon followed by the oxidation, for which the weight increase was recorded. These measurements were performed with high purity argon (99.9995) (PanGas, Switzerland) and with artificial air (20.95% of oxygen, 99.9995).

3. Results

In Table 3 the nominal compositions of produced powders and their denotations are summarized. In general, so-called understoichiometric compositions of $La_{0.2}Sr_{0.7}TiO_3$ are produced by a solid state route (Batch LST_{SSR}) and by a nanoparticle based spray pyrolysis (NSP, Batches LST_{27}). For reasons discussed below, two further batches of $LST_{27\text{-}04}$ and $LST_{27\text{-}06}$ were produced, which contain slightly higher amounts of Sr.

3.1. LST produced by solid state reaction (SSR)

The solid state route represents the simplest and the most widely used technique for powder production of lanthanum doped strontium titanates (LSTs). Fig. 2 shows the XRD patterns of the SSR powder (Batch LST_{SSR1}) after calcination for 20 h at different temperatures. Fig. 2 also includes the Bragg position of cubic LST

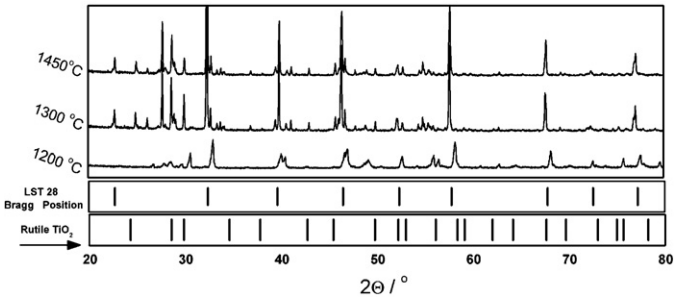

Fig. 2. XRD patterns from LST-powders prepared with SSR calcined for 20 h at 1200 °C to 1450 °C. Bragg positions of $SrTiO_3$ (LST28) (JCPDS card No. 86-179) and TiO_2 (rutile) (JCPDS card No. 88-1172) are given as a guide to the eye at the bottom. Note that not all of the reflections have been marked to maintain the clarity on the figure. Unmarked patterns represent pyrochlore $La_2Ti_2O_7$ and various La–Sr–Ti stoichiometries.

$La_{0.2}Sr_{0.8}TiO_{3+\delta}$ as a reference (JCPDS card No. 86-179). All patterns from LST_{SSR1} contain peaks which indicate the existence of secondary phases. Hence, no single phase powder of LST could be achieved with SSR, even not after heat treatments at 1200 °C, 1300 °C and 1450 °C for 20 h. The appearance of secondary phases becomes more pronounced, when calcinations are carried out at higher temperatures of 1300 °C and 1450 °C. In addition, a peak shift of the primary perovskite was found in the XRD-spectra at higher temperatures. The peaks of the secondary phases can be assigned to TiO_2 (rutile), $La_2Ti_2O_7$ and different La–Sr–Ti oxides with variable stoichiometry. These XRD results indicate that an up-scaled powder production of phase pure LST is difficult to be achieved with SSR. Therefore, in the further investigations we are focusing on a more promising approach with nanoparticle based spray pyrolysis (NSP) in order to overcome the obvious diffusion problems that seem to be inherent to the SSR powders.

3.2. LST produced by nanoparticle based spray pyrolysis (NSP)

The LST powders produced by nanoparticle based spray pyrolysis (NSP) have a significantly lower amount of secondary phases than those produced by SSR. Thereby it was noticed from earlier experiments that the application of submicron sized rutile (TiO_2) as a precursor results in a particularly high phase purity. Two different materials, an understoichiometric composition ($La_xSr_{1-1.5x}TiO_{3+\delta} = LST_{27}$) and an understoichiometric composition with a slight enrichment of Sr (i.e. $La_xSr_{1-1.5x+x}TiO_{3+\delta} = LST_{27\text{-}04}$ and $LST_{27\text{-}06}$) are described separately in the following sections. The morphology and the characterisation of as-prepared powders are discussed in general since it is very similar for all these compositions.

3.2.1. General powder characteristics of NSP materials

Fig. 3 shows STEM images of LST from NSP production in the 'as-prepared' state (left) and after calcination including a grinding step (right). In the as-prepared state the primary particle size

Table 3
Specifications of produced LST-powders, including the corresponding nomenclature, stoichiometry, specific surface area (SSA) from BET-measurements and phase purity after thermal treatment.

Nomenclature of produced materials	Nominal stoichiometric compositions	La to Sr ratio	Production technique	Specific surface area ($m^2\ g^{-1}$) from 'as prepared powders'	Phase purity after thermal treatment
LST_{SSR}	$La_{0.2}Sr_{0.7}TiO_3$	0.2:0.7	SSR	7.2	Secondary phases
LST_{27}	$La_{0.2}Sr_{0.7}TiO_3$	0.2:0.7	NSP	16	Single phase
$LST_{27\text{-}04}$	$La_{0.2}Sr_{0.704}TiO_{3+\delta}$	0.2:0.704	NSP	16.8	Single phase
$LST_{27\text{-}06}$	$La_{0.2}Sr_{0.706}TiO_{3+\delta}$	0.2:0.706	NSP	17.1	Single phase

SSR: solid state route reaction; NSP: nanoparticle based spray pyrolysis.

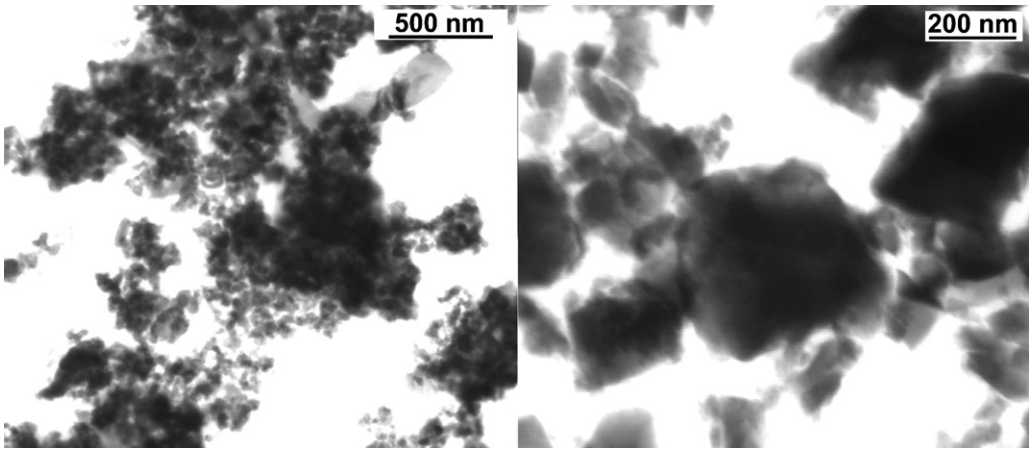

Fig. 3. STEM bright field images of LST powders from spray pyrolysis (NSP) showing particle size and morphology: left, nano-sized powder before calcination (17 $m^2\,g^{-1}$); right, bimodal powder after calcination and subsequent grinding (13 $m^2\,g^{-1}$).

measured from STEM images is in the range of 30–50 nm. This corresponds well with the monosized spherical diameter (d_{50BET}) of 47 nm which is calculated from the measured specific surface area (SSA_{BET}) of 17 $m^2\,g^{-1}$. The STEM images also illustrate that the as-prepared powder has a narrow size distribution.

After calcination a surface area (SSA) of approximately 2 $m^2\,g^{-1}$ (d_{50BET} = 554 nm) is received, which can be increased up to 13 $m^2\,g^{-1}$due to additional grinding. The corresponding STEM image documents that a bimodal size distribution is obtained after calcination and regrinding. For this specific powder the SSA of 13 $m^2\,g^{-1}$corresponds to an average equivalent diameter (d_{50BET}) of 86 nm. High energy planetary milling results in powders with higher specific surface area (SSA) up to 21 $m^2\,g^{-1}$ (d_{50BET} = 55 nm).

3.2.2. Characterisation of understoichiometric $La_xSr_{1-1.5x}TiO_3$ (Batch LST_{27})

3.2.2.1. Effect of sintering temperature on phase purity. The material with a nominal composition of $La_{0.2}Sr_{0.7}TiO_3$ (LST_{27}) was investigated by XRD and SEM. Fig. 4 shows results from X-ray diffraction for different calcination temperatures. All XRD spectra are normalized to the LST main reflection (1 1 0). In general the phase purity is much higher compared to the SSR powders. Already a temperature treatment of 1200 °C for 5 h resulted in a powder where the main perovskite structure has formed (Fig. 4a). All powders produced at 1200 °C showed minimal reflections of rutile (TiO_2), which could not be eliminated by additional annealing up to 12 h. Powders calcined at 1250 °C show a single phase XRD pattern of cubic perovskite (Fig. 4b). Further increment of the temperature to 1300 °C led to re-appearance of TiO_2-traces (Fig. 4d and e) and possibly of some pyrochlore ($La_2Ti_2O_7$) (Fig. 4c). Overall the comparison of XRD analyses at increasing calcination temperatures indicates a temperature window, where phase purity of the spray pyrolysed $La_{0.2}Sr_{0.7}TiO_3$ is maintained. This temperature window was found between 1250 °C and 1300 °C. Below 1250 °C the formation of the perovskite phase is not yet pronounced enough, while above 1300 °C progressive phase segregation and formation of secondary phases are observed.

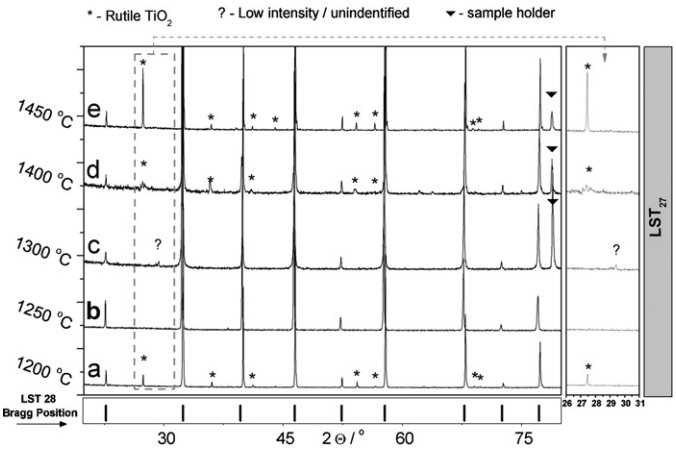

Fig. 4. XRD patterns as a function of calcination temperature for two spray pyrolysed batches (LST_{27}) with a nominal composition of $La_{0.2}Sr_{0.7}TiO_3$. Bragg positions of $SrTiO_3$ are given as a guide to the eye (JCPDS card No. 86-179). *Legend*: Star, rutile TiO_2; question mark, unidentified phase; triangle, sample holder.

Interstitial domains of a distinct dark grey phase (Fig. 5) appear in the SEM/BSE images from LST samples sintered at 1400 °C and at 1450 °C. It was confirmed by EDX analysis that the dark grey phase is TiO_2 (rutile). The specimen sintered for 90 min at 1450 °C shows large spherical LST grains (about 20–28 μm in size). The dark Ti-rich phase is localized at the interstices between the grain boundary junctions of the large LST grains. The larger grain size and the higher amount of secondary rutile which appears at slightly higher temperatures in the SEM images (compare Fig. 5, left and right) is in a good agreement with a higher intensity of rutile that is observed in the corresponding XRD spectra (compare Fig. 4e). Hence, this indicates that at higher temperatures more secondary phases are formed.

3.2.2.2. Electrical conductivity of phase impure $La_xSr_{1-1.5x}TiO_3$ (Batches LST_{27}). In Fig. 6 the temperature dependence of conductivity is shown for three LST_{27} samples with different sintering temperatures. All three measurements are performed under reducing conditions of forming gas. The effect of the sintering temperatures is illustrated by a comparison of curve 1 (NSP_{27}, 1450 °C), curve 2 (NSP_{27}, 1400 °C), and curve 3 (NSP_{27}, 1250 °C). The sample sintered at higher temperatures (curve 1) has a relatively low conductivity of 2.66 S cm^{-1} at 930 °C compared to 4.59 S cm^{-1} in curve 2. The highest conductivity (23 S cm^{-1}) was measured for a specimen that was sintered at 1250 °C. As shown above (see Figs. 4 and 5), the different sintering temperatures also lead to microstructural changes associated with coarsening of LST and even pronounced formation of secondary rutile. The decrease of conductivity with increasing sintering temperatures can thus be correlated with microstructure coarsening and accompanying formation of secondary phases.

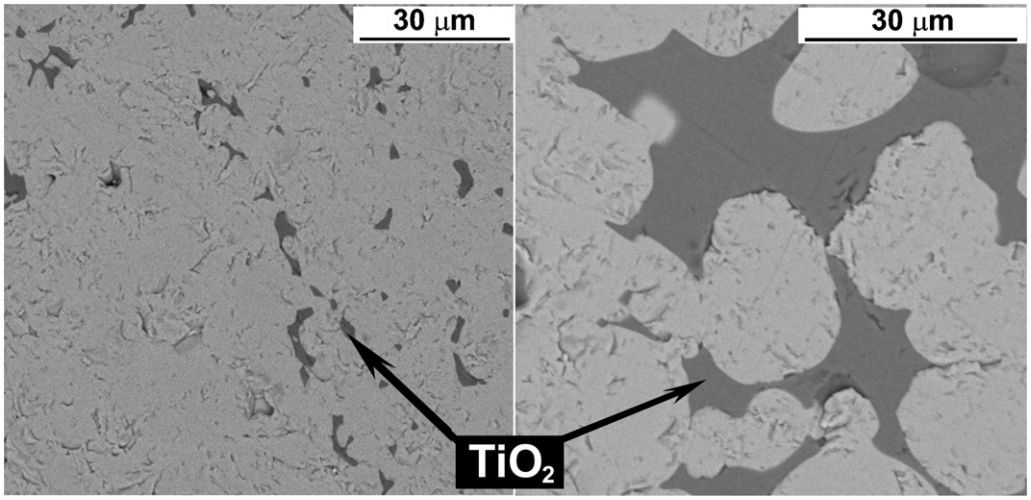

Fig. 5. SEM images with backscatter contrast (BSE) of LST_{27} sintered at 1400 °C (left) and at 1450 °C (right). Dark grey domains represent interstitial TiO_2 whereas the bright grey matrix is attributed to LST. *Right*: A magnified area, which is not representative for the whole material. It shows a local area, where the concentration of secondary TiO_2 is enriched.

3.2.3. Characterisation of Sr-enriched understoichiometric $La_xSr_{1-1.5x+ax}TiO_{3+\delta}$

3.2.3.1. Effect of calcination temperature on phase purity (Batches $LST_{27\text{-}04}$ and $LST_{27\text{-}06}$). Two LST compositions with a slight Sr-enrichment (0.02 and 0.03 per formula unit) were produced in order to study the effect of a compositional variation on the material properties and phase stability. Fig. 7 illustrates the temperature dependence of secondary phase formation, in analogy to Fig. 4. Powders of $LST_{27\text{-}04}$ calcined at 1200 °C show traces of secondary phases (Fig. 7) similarly to the LST_{27} (Fig. 4a and e). The temperature window, for which the cubic structure and phase purity are retained, is between 1250 °C and 1450 °C. The Sr-enriched material denoted as $LST_{27\text{-}04}$ reaches phase purity at 1250 °C (Fig. 7c) while $LST_{27\text{-}06}$ needs almost 100 °C higher temperatures (Fig. 7h). Apparently a larger enrichment of Sr requires higher temperatures of calcination in order to reach phase purity. In contrast to the above-described productions of LST_{27}, both enriched compositions of $LST_{27\text{-}04}$ and $LST_{27\text{-}06}$ manifest improved phase stability at elevated temperatures without secondary phase formation up to 1450 °C and 1500 °C, respectively. A slight addition of Sr thus leads to a stabilization of the understoichiometric LST structure at higher temperatures (above 1250 °C).

3.2.3.2. Electrical conductivity of single phase Sr-enriched understoichiometric $La_xSr_{1-1.5x+ax}TiO_{3+\delta}$ (Batch $LST_{27\text{-}04}$). Fig. 8 shows the temperature dependency of the conductivity in Sr-enriched understoichiometric $LST_{27\text{-}04}$ sintered at 1250 °C in air and subsequently reduced at different temperatures (24 h at 980 °C + 1 h at T_{RED}). Thereby significantly different conductivities are obtained depending on the final pre-reduction temperature (T_{RED}). The maximum conductivity is increasing from 106 S cm^{-1} (T_{RED} 980 °C) to 159 S cm^{-1} (T_{RED} 1100 °C), 392 S cm^{-1} (T_{RED} 1150 °C) and 2051 S cm^{-1} (T_{RED} 1200 °C), respectively. At the same time also the temperature ($T_{OPERATING}$) corresponding to the maximum conductivity is slightly shifted with the reduction temperature from 225 °C (T_{RED} 980 °C) to 274 °C (T_{RED} 1200 °C). It is assumed that the increase of conductivity at higher reduction temperatures is associated with an increase of the ratio Ti^{3+}/Ti^{4+} due to a stronger

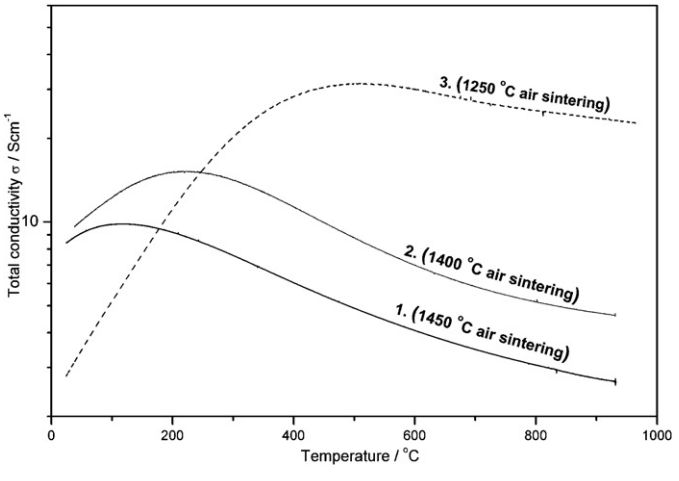

Fig. 6. Temperature dependent conductivity of LST_{27} sintered for 90 min at three different sintering temperatures. *Legend*: 1. LST_{27} sintered at 1450 °C in air; 2. LST_{27} sintered at 1400 °C; 3. LST_{27} sintered at 1250 °C for 16 h. All samples were isothermally reduced at 980 °C in forming gas (5% H_2 in N_2) and subsequently cooled down to room temperature while monitoring the conductivity. The total gas flow corresponds to 250 ml min^{-1}.

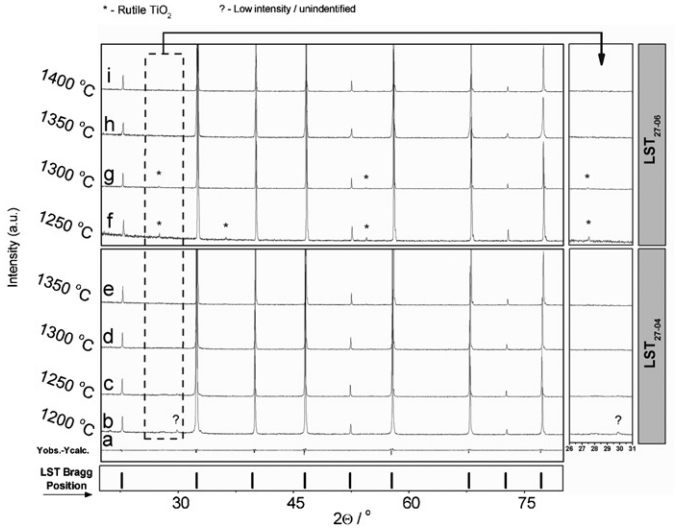

Fig. 7. Normalized XRD patterns as a function of the calcination temperature for Sr-enriched understoichiometric compositions $LST_{27\text{-}04}$ and $LST_{27\text{-}06}$. Bragg positions of $SrTiO_3$ are given as a guide to the eye (JCPDS card No. 86-179) at the bottom. *Legend*: Star, rutile TiO_2; question mark, unidentified phase.

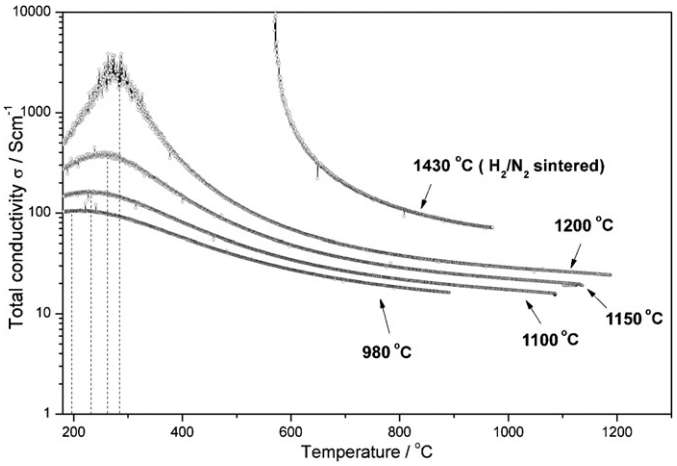

Fig. 8. The temperature dependence of conductivity in Sr-enriched understoichiometric LST_{27-04}. All samples were sintered in air at 1250 °C for 16 h and subsequently reduced at 980 °C for 24 h in dry 5% (N_2/H_2) forming gas followed by further pre-reduction for 1 h at different temperatures (T_{RED}, as indicated in the figure).

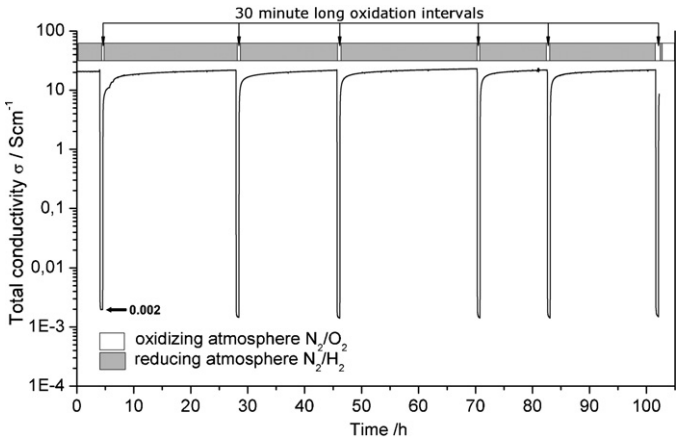

Fig. 10. Isothermal redox cycling at 980 °C ($T_{OPERATING}$) of air sintered LST_{27-04}. Before the measurement the reduction was lasting 24 h at 980 °C (T_{RED}). Note, that each 30 min long oxidation step has led to a complete loss of conductivity (0.002 S cm^{-1}). The image modified from Ref. [39]. The nitrogen flux with 250 ml min^{-1} was applied for 1 min before each oxidation and reduction cycle.

reduction (according to Eq. (6)). The shift of conductivity values documented in Fig. 8 indicates that the degree of reduction is strongly dependent on the final reduction temperature (T_{RED}).

In Fig. 9 (top) the electrical conductivity is shown as a function of T_{RED} (*x*-axis) for dense, Sr-enriched understoichiometric LST specimens. Thereby each curve represents the measured conductivities at a given operating temperature ($T_{OPERATING}$). The reduction performed for 24 h at 980 °C resulted in a conductivity of 16 S cm^{-1} at 930 °C ($T_{OPERATING}$) and 28 S cm^{-1} at 600 °C. Further pre-reduction for 1 h at T_{RED} of 1100 °C, 1150 °C, 1200 °C and 1430 °C gave a rise to enhanced conductivity of 19 S cm^{-1}, 24 S cm^{-1}, 31 S cm^{-1} and 71 S cm^{-1} (at 930 °C $T_{OPERATING}$), respectively. Simultaneously the cubic lattice parameter '*a*' shows continuous expansion with increasing reduction temperature, as shown in Fig. 9, bottom. This expansion can be attributed to increasing ratio Ti^{3+}/Ti^{4+} upon reduction. Thereby Ti^{3+} has a larger ionic radius than Ti^{4+}. A reduction period of 6 h at 1430 °C resulted in the highest lattice value of 3.911(0), which corresponds to a relative expansion of 0.38%. It has to be noted, that the curve describing the lattice expansion has an asymptotic shape, whereby the lattice parameter hardly increases above 1400 °C. Therefore, it can be concluded that the material sintered at 1430 °C experienced severe reduction conditions and approaches the upper limit of the Ti^{3+} concentration.

The change of mass during oxygen uptake according to Eq. (1) was measured for a specimen sintered at 1430 °C in forming gas after calcination at 980 °C. The reduced sample was analysed with thermogravimetry under oxidizing atmosphere whereby a mass increase of 0.81% was measured. The amount of incorporated oxygen corresponds to the concentration of trivalent Ti^{3+} (see Eq. (1)) which will be discussed below.

3.2.3.3. Reduction–oxidation kinetics of single phase Sr-enriched understoichiometric $La_xSr_{1-1.5x+ax}TiO_{3+\delta}$ (Batch LST_{27-04}). In Fig. 10 the redox cycling of LST_{27-04} performed over a period of 120 h is shown. The introduction of the oxidizing atmosphere results in an immediate loss of conductivity and therefore quick response to the change of oxygen partial pressure. It was found that within 2 h of reduction 95% of the initial conductivity is restored and after 12.5 h 100% of conductivity is restored. All redox cycles have led to fully reproducible conductivity values and reached nearly steady-state under the given experimental conditions. After 6 cycles the initial conductivity could be recovered, which proves that the overall redox-stability of this material is very good.

Fig. 11 represents a comparison of the redox-kinetics of LST_{27} (with TiO_2 secondary phases) and LST_{27-04} (single phase). The presence of the secondary phases and large grains in the material remarkably slows down the overall reaction kinetics upon a change

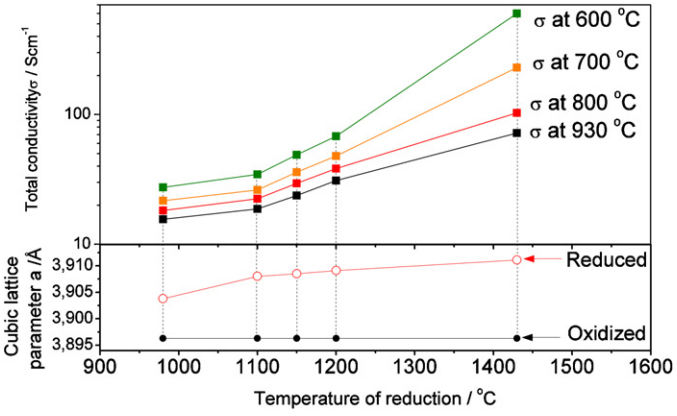

Fig. 9. *Top*: Influence of reduction temperature (T_{RED}) on the conductivity of Sr-enriched understoichiometric LST_{27-04} at different operating temperatures ($T_{OPERATING}$). *Bottom*: Gradual change of cubic lattice parameter "*a*" as a function of increasing reduction temperature.

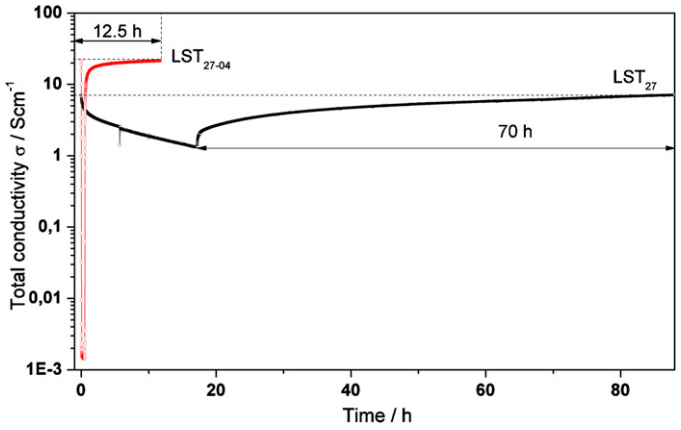

Fig. 11. Comparison of a single redox cycle for LST_{27} (containing secondary phases) and LST_{27-04} (single phase). Both cycles were performed at 980 °C. Initial conductivity was restored after 12.5 h for LST_{27-04} and after 70 h for LST_{27}.

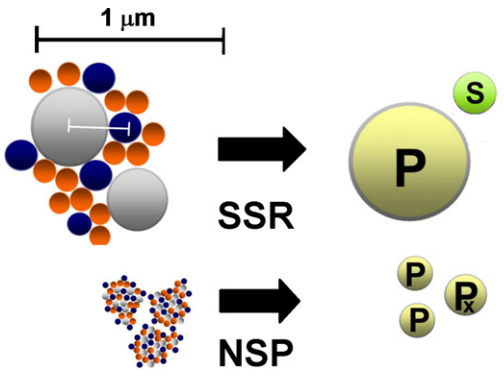

Fig. 12. A schematic illustration of the phase formations with the two synthesis routes (SSR and NSP). Note that the use of nanoparticles in NSP leads to shorter diffusion path lengths which is important for the synthesis of a phase pure LST powder. *Legend*: P, desired perovskite phase; S, secondary phase; P_x, perovskite phase with slightly deviating stoichiometry.

of oxygen partial pressure. The single phase material shows at least 6 times faster response to both oxidizing and reducing atmosphere. Thereby with the single phase materials a higher conductivity could be achieved within much shorter reaction period after reoxidation.

4. Discussion

4.1. Comparison of $La_{0.2}Sr_{0.7}TiO_3$-productions with solid state reaction (SSR) and with spray pyrolysis (NSP) techniques

In the XRD results presented in Fig. 2 it can be observed, that LST_{27} from SSR decomposes at temperatures higher than 1300 °C, which leads to relatively high amounts of secondary phases compared to the LST_{SSR} that was calcined at 1200 °C. However, the powder calcined at 1200 °C does not show a well crystalline $La_{0.2}Sr_{0.7}TiO_3$ phase. From these observations it can be concluded that the diffusion kinetics of La and Sr into the titanate lattice is too slow at 1200 °C for an efficient phase formation (see Fig. 12). In order to increase the diffusion kinetics the temperature has to be raised to 1300 °C or even higher. But this temperature rise leads again to additional problems related to secondary phases—presumably because the decomposed phase (mainly TiO_2) blocks the diffusion of La and Sr into the perovskite structure.

Thus, in order to obtain a phase pure LST powder with the SSR technique, significantly longer annealing times of a fine submicron powder at temperatures lower than 1300 °C are required. However, longer annealing times lead to coarser grains and therefore grinding and annealing in a repetitive procedure as reported in the literature [31] has to be carried out in order to achieve a phase pure and fine grained LST powder. Such a time consuming and costly procedure limits the suitability of the SSR technique and makes it inefficient for the production of larger LST batches, which are required for practical applications such as electrode fabrication for SOFCs.

In contrast to the SSR technique, LST powders with a lower amount of secondary phases or even phase pure powders could be prepared with the NSP technique. Very short annealing times of 5–10 h and much lower temperatures of 1250 °C are necessary to form a single phase $La_{0.2}Sr_{0.7}TiO_3$ powder due to much shorter reaction pathways, as it is schematically shown in Fig. 12 for the NSP route. This effect is attributed to the presence of nano-range TiO_2 particles that are still present after the pre-calcination step. The preservation of nano-scale rutile and associated short diffusion path length thus seems to be crucial for the synthesis of single phase $La_{0.2}Sr_{0.7}TiO_3$.

When comparing the XRD results from different productions, identical lattice parameters are considered as an indicator for the similarity of understoichiometric and A-site deficiency. Table 4 summarizes the lattice parameters of the aimed $La_{0.2}Sr_{0.7}TiO_3$ and the corresponding information about the production routes from LST investigations reported in literature. Overall, the lattice parameters from successful SSR productions in literature are very similar as the ones obtained in this study by means of the NSP technique. However, with the NSP-method already a phase pure LST powder can be obtained at relatively low calcination temperatures of only 1250 °C. The corresponding XRD patterns were refined as a cubic Pm-3m structure (2 2 1) and they exhibit the perovskite structure similar to the standard XRD pattern of undoped $SrTiO_3$ (JCPDS card No. 86-179). With increasing calcination temperature the cubic lattice parameter tends to decrease slightly. Those lattice parameters obtained from the NSP-produced LST correspond well to the available literature data of $La_{0.2}Sr_{0.7}TiO_3$ as shown in Table 4. It is worth to mention that with the SSR production single-phase materials can only be obtained by a repetitive grinding-annealing procedure, while in the present study phase pure $La_{0.2}Sr_{0.7}TiO_3$ powders can be obtained after a single calcination step with the NSP-technique. This simplifies the entire powder processing and significantly reduces the costs of production and enables the efficient synthesis of larger LST batches.

Spray pyrolysis is a long time established method for complex multi-elemental ceramics and is an easily up-scalable process. The largest batch of LST produced via NSP for this in house research activity was 2 kg within one day, but can be more than doubled if necessary. That powder quantities are already far beyond a typical laboratory approach for ceramic oxide production. The limitations of NSP daily productions are primarily caused by the size of employed spray pyrolysis setup (i.e. size of the chamber, uniformity of the temperature regimes) and the necessity of further temperature treatment application.

4.2. Influence of Sr enrichment on the phase stability of LST_{27}

As shown by XRD (see Fig. 4) the understoichiometric LST_{27} shows a limited stability at elevated temperatures (>1300 °C). Similar to observations made on some other understoichiometric compositions [33,34] this material tends to undergo a liquid phase sintering, whereby an intergranular TiO_2 phase is formed (see SEM images in Fig. 5). A better phase stability and a lower tendency to form secondary phases at temperatures > 1300 °C could be achieved with a slight enrichment of the Sr content of about 0.04–0.06 mol% ($La_{0.2}Sr_{0.7+ax}TiO_{3+\delta}$, Batches $LST_{27\text{-}04}$ and $LST_{27\text{-}06}$). The careful analysis of XRD-diffractograms indicates that the appearance of titania as a secondary phase is depending on temperature as well as on the strontium content. The relation between the strontium content and the calcination temperature at which the corresponding LST composition could be processed as a single phase material is illustrated in Fig. 13. As discussed above, the relatively large diffusion path lengths in the particles, present in the SSR production, require firing temperatures above 1300 °C, which result in the formation of secondary phases ($La_2Ti_2O_7$ and TiO_2). The data in Fig. 13 indicate that a slight increase of the Sr-content will stabilize the understoichiometric LST at elevated temperatures. This effect is particularly important for the SSR-production route, which requires higher firing and calcination temperatures than the NSP-technique.

The XRD-patterns (Figs. 2, 4 and 7) and the corresponding SEM images (Fig. 5) document that the sintering of understoichiometric LST tends to undergo intensive grain growth and formation of a secondary TiO_2 phase. Hence, it appears that a Ti-rich phase is preferably exsolved from deficient LST-perovskites. The findings of our study on the stability of A-site deficient $(La,Sr)TiO_3$ are in agreement with previous investigations that can be summarized as follows:

Table 4
Summary of lattice parameters for LST_{27} powders produced with the SSR technique from literature and comparison with XRD-data from LST_{27} produced with the NSP technique (this study).

Synthesis route	Firing temp. (°C)	Dwelling time [h]	Lattice parameter, a (Å)	Ref.
SSR	1400	4, multi-step	3.897	[34]
SSR	1400	10, multi-step	3.8973	[35]
SSR	1440	24, multi-step	3.9014	[24]
SSR	1450	12, multi-step	3.8959	[15]
NSP	1250	5, single-step	3.903(6)	This work
NSP	1310	10, single-step	3.900(6)	This work
NSP	1350	10, single-step	3.897(4)	This work

Note: Multi-step = repeated grinding and annealing; single-step = single calcination step.

(I) The undoped $SrTiO_3$ is unlikely to exist as a highly deficient single phase perovskite in oxidizing atmospheres. It was shown [40–44] that the maximum deficiency of Sr in phase pure $SrTiO_3$ is lower than 0.02 mol%.
(II) The stability of A-site deficient strontium titanate is increased by addition of La as a donor dopant [32–34].
(III) A slight strontium enrichment of about 0.01 in the nominal formula reduces the tendency for liquid phase sintering in deficient lanthanum doped $SrTiO_3$ [33,34]. In order to stabilize the perovskite structure, approximately 2 mol% of La is needed to compensate 1 mol% of Sr vacancies and excess of titania, respectively.

The formation of A-site deficient lanthanum strontium titanate can be described as a solution of $La_{2/3}TiO_3$ in $SrTiO_3$. The x variable represents the actual strontium content:

$$(1-y)Sr_xTiO_3 + yLa_{2/3}V_{1/3}TiO_3 \rightarrow La_{(2/3)y}Sr_{x(1-y)}V_{(1/3)y}TiO_3; \quad V: \text{ vacancy.} \tag{9}$$

Since the maximum deficiency of $SrTiO_3$ is lower than 0.02 mol%, it follows that x_{min} is 0.99. To introduce 20 mol% of La (for composition $La_{0.2}Sr_{0.7}TiO_3$) and 10 mol% of vacancies the "y" will be equal to 0.3:

$$La_{0.2}Sr_{x0.7}V_{1-0.2-x0.7}TiO_3 \rightarrow La_{0.2}Sr_{0.693}V_{0.107}TiO_3. \tag{10}$$

If this composition is fired at temperatures below 1290 °C the maximum amount of Sr-vacancies is 0.107 on the A-site. The difference between the actual strontium content and the deficiency limit of x_{min} = 0.99 represents the number of moles which will theoretically be exsolved as free titania. The understoichiometric LST compositions are on the miscibility limit of the cation vacancies. As a consequence, small compositional variations in the perovskite material such as locally concentrated titania or locally depleted La and Sr may induce phase segregation. The XRD results indicate that in LST_{27} this process occurs preferably at temperatures higher than 1290 °C. In literature it is described that such slight compositional variations may occur in the as-prepared powders due to physical phenomena that take place during the pyrolysis [45–47]. Thereby, it is highly probable that strontium, which has a rather low solubility in the used solvents, will precipitate on the outer surface of aerosol droplets [48,49] or on the titania particles, due to their high surface energy [50–53]. Based on these considerations it can be argued that the addition of small amounts of Sr efficiently prevents the formation of free TiO_2 and thus enhances the stability at higher temperatures.

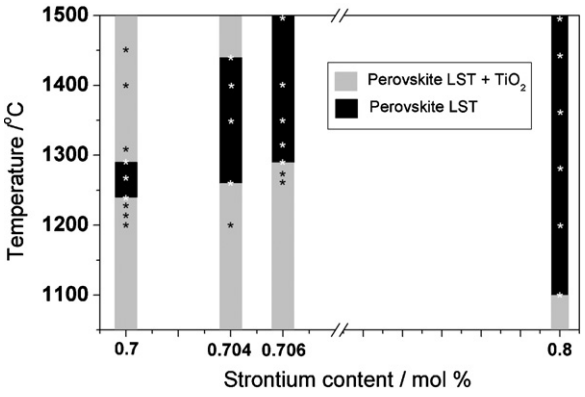

Fig. 13. Phase stability as indicated from XRD-data as a function of firing temperature and strontium content. Note that the stability of the stoichiometric $La_{0.2}Sr_{0.8}TiO_3$ composition (Sr content of 0.8) is known from ongoing studies (unpublished data). *Firing temperatures of samples from which XRD was collected at room temperature.

4.3. *Electronic properties of $La_{0.2}Sr_{0.704}TiO_3$ (LST_{27+ax} with slight enrichment of Sr)*

As explained in Section 1, the performance of understoichiometric lanthanum strontium titanates is driven by the change of oxidation state from Ti^{4+} toTi^{3+} upon reduction and by the corresponding defect chemistry (see Eqs. (1), (2), (7) and (8)). The concentration of reduced Ti^{3+} and the associated conductivity are strongly influenced by the reduction conditions (see Fig. 8). For example, for $La_{0.2}Sr_{704}TiO_3$ a relatively high conductivity of 71 S cm^{-1} (at 930 °C $T_{OPERATING}$) could be achieved for T_{RED} of 1430 °C, whereas a T_{RED} of only 980 °C resulted in a significantly lower conductivity of 16 S cm^{-1} (at 930 °C $T_{OPERATING}$). Furthermore it was observed that $La_{0.2}Sr_{704}TiO_{3+\delta}$ is reacting relatively fast upon a change of pO_2 as it observed during redox cycling in Fig. 10. Hence, the electrical conductivity and the redox kinetics of understoichiometric LST, as documented in the present study, differ significantly from the corresponding properties of stoichiometric $La_{0.2}Sr_{0.8}TiO_{3+\delta}$. For the latter, stoichiometric material slow redox kinetics and significantly lower conductivities are described in literature [13].

It can be assumed that these materials properties of the different LST-types are strongly related to their distinct defect chemistries. The expected defect chemistry of $La_{0.2}Sr_{0.704}TiO_{3+\delta}$ under oxidizing conditions can be described as follows:

$$0.2La_{Sr}^{\bullet} + 0.704Sr_{Sr}^{x} + 0.096V_{Sr}^{\bullet\bullet} + Ti_{Ti}^{x} + 3O_{O}^{x} + 0.004O_{i}'' . \tag{11}$$

According to Eqs. (7) and (8), the excess charge from trivalent lanthanum in understoichiometric LST is fully compensated by the formation of strontium vacancies and does not include Ti-reduction. Since the small concentration of interstitial oxygen ($0.004O_i''$) can be neglected, the concentration of Ti^{3+} is then mainly related to the oxygen removal from the perovskite lattice which takes place under reducing conditions. As proposed by Hui et al. the A-site vacancies have a strong influence on the reduction kinetics by weakening the Ti–O–Ti bond strength within the TiO_6 octahedra that are localized around these vacancies [25]. Hence, the concentration of Ti^{3+} and the corresponding conductivity are not directly influenced by the concentration of donor

dopants. However, the lanthanum doping and the associated presence of strontium vacancies enhance the conductivity in an indirect way, namely by distortion effects in the perovskite lattice. A large number of strontium vacancies will thus lead to enhanced oxygen removal and associated higher Ti-reduction and conductivity, what is supported by the findings of previous investigations independent from the production route. For example Savaniu [15] reported a fast reduction kinetics for phase pure $La_{0.2}Sr_{0.7}TiO_{3+\delta}$, which was prepared by SSR on a small laboratory scale.

In contrast to some studies in literature, from our investigations there is no evidence for extended oxygen defects (i.e. linear defects or layered crystal rearrangements) in the understoichiometric $LST_{27\text{-}04}$. Firstly, the cubic lattice parameter "*a*" presented in Fig. 9 (bottom) shows a continuous lattice expansion upon the increase of the reduction temperature. This phenomenon is undoubtedly the result of the valence change on the B-site and of the associated change in ionic radii (Ti^{4+} = 0.68 Å, Ti^{3+} = 0.81 Å [54], for a 8-fold coordination). Secondly, the data from thermogravimetry of $La_{0.2}Sr_{0.704}TiO_{3+\delta}$ (T_{RED} 1430 °C) show a mass increase during re-oxidation of 0.81%. According to Eq. (1) the amount of trivalent titanium, necessary to compensate the charges involved with the measured oxygen removal under reducing conditions can be determined, which is approximately 17–18% of the total titanium. This indirectly measured concentration of Ti^{3+} is very close to the nominal La-doping level of 20 mol%. Hence, in contrast to $La_{0.2}Sr_{0.8}TiO_3$, the vacancy compensation mechanism of understoichiometric LST does not necessitate the formation of extended oxygen defects. In stoichiometric LST these extended defects strongly interrupt the electron hopping mechanism between adjacent B-site ions. The absence of those defects in the understoichiometric LST may explain why the electrical performance of $LST_{27\text{-}04}$ is remarkably higher than in the stoichiometric LST.

4.4. Electronic properties of $La_{0.2}Sr_{0.7}TiO_3$

As displayed in Fig. 6, the increase of the sintering temperature in air leads to a drop of conductivity in LST_{27}. Correspondingly, formation of interstitial secondary phases is observed by SEM (see Fig. 4d and e) at temperatures above 1300 °C. The presence of these secondary phases cannot easily be taken as an explanation for the observed drop in conductivity, since the LST matrix forms a percolating network, where the electrical current is not significantly hindered by the interstitial grains. Nevertheless, the XRD-analyses confirm that there is a correlation between the formation of secondary phases and the decrease of conductivity. At the same time slow oxygen migration for TiO_2 containing phases can be assumed based on the slow redox kinetics, which was observed in samples with secondary titania. The formation of secondary phases may thus induce several overlapping and interfering effects on the macroscopic material properties, as discussed in the following.

The exsolution of Ti from the B-site leads to a change of the nominal stoichiometry towards LST compositions with lower deficiency:

$$La_xSr_{1-1.5x}TiO_{3+\delta} \xrightarrow{Temp} La_{x(1+y)}Sr_{(1-1.5x)(1+y)}Ti_{(1-y)}O_{3+0.5xy} + yTiO_2. \quad (12)$$

Hence, the exsolution of a Ti-rich secondary phase results in a higher La content, which may induce a change of the charge compensation mechanism and associated materials properties such as the redox kinetics. It was reported that for LST with high La contents above 20 mol% a lower pO_2 atmosphere is required in order to obtain the same conductivity which is otherwise obtained for LST with lower La contents [8,24,55]. The change of the nominal composition thus might contribute to the observed decrease of conductivity associated with the formation of secondary phases.

In summary the results illustrate that the bulk properties of LST-samples may be affected significantly by even minor contents of secondary phases. It is thus assumed that the stoichiometry of the LST and the defect structures are influenced by secondary phase formation. Consequently a careful evaluation of the crystal structure and of the phase stability is very important in order to guarantee reproducible and high quality material properties.

5. Conclusions

It is shown that a modified spray pyrolysis process, denoted as nanoparticle based spray pyrolysis is a suitable and versatile technique for medium to large scale production for phase pure lanthanum doped strontium titanate powders. A-site deficient $La_{0.2}Sr_{0.7}TiO_3$ was successfully produced from a mixture of colloidal titania and nitrate salts. Such a process is a low-cost powder production technique, which overcomes the drawbacks of high temperature calcination and long dwelling time necessary to achieve the single phase material. Lower temperatures of single phase perovskite formation than those typically used for the solid state reaction route are attributed to the presence of nano-scale titania particles in the precursor.

The current investigation shows that LST with the stoichiometry of $La_{0.2}Sr_{0.7}TiO_3$ has limited phase stability at temperatures above 1290 °C. Marginal Sr-addition of about 0.02 ($La_{0.2}Sr_{0.704}TiO_{3+\delta}$) to 0.03 ($La_{0.2}Sr_{0.706}TiO_{3+\delta}$) per formula unit significantly enhances the phase stability for temperatures up to 1500 °C. Limited solubility of excessive TiO_2 in $SrTiO_3$ is identified as a critical factor, because the formation of secondary phases strongly affects the electrical conductivity and the redox-behaviour.

Conductivities of air sintered LST illustrate that deficient LST can be applied for intermediate and high temperature fuel cells due to its n-type conductivity. A material preparation under moderate reducing atmosphere ($pO_2 = 10^{-21}$) at 980 °C has provided conductivity values as high as 24 S cm^{-1} at 930 °C. Progressive harsher pre-reduction conditions for 1 h at 1100 °C and 1200 °C resulted in much higher conductivities. A reductive sintering at 1430 °C gave a rise to impressive conductivity of 71 S cm^{-1} at 930 °C and 600 S cm^{-1} at 600 °C. Air-sintered $La_{0.2}Sr_{0.704}TiO_{3+\delta}$ have shown fully reproducible conductivity values within 12 h and can be considered as potential redox stable material. Simultaneously, the oxygen reduction kinetics of deficient titanate was found to be very sensitive to minor secondary phase contents. The reason for this needs detailed study.

Acknowledgements

The authors would like to gratefully acknowledge the Swiss SCIEX-NMS^{CH} fellowship programme (No. PL0908005) for financial support. The authors would also like to thank Dr. Eugenio Otal for performing high quality thermogravimetry analyses and to Dr. Lassi Karvonen for many fruitful discussions.

References

[1] A.L. Dicks, J. Power Sources 61 (1996) 113–124.
[2] A. Weber, B. Sauer, A.C. Muller, D. Herbstritt, E. Ivers-Tiffe, Solid State Ionics 152–153 (2002) 543–550.
[3] D. Sarantaridis, A. Atkinson, Fuel Cells 7 (2006) 246–258.
[4] L. Holzer, B. Iwanschitz, J. Power Sources 196 (2010) 1279–1294.
[5] J.-M. Klein, S. Georges, Y. Bultel, J. Electrochem. Soc. 155 (2008) B333–B339.
[6] B. Iwanschitz, J. Sfeir, A. Mai, M. Schutze, J. Electrochem. Soc. 157 (2010) B269–B278.
[7] P. Holtappels, U. Vogt, T. Graule, Adv. Eng. Mater. 7 (2005) 292–298.
[8] X. Li, H. Zhao, N. Xu, X. Zhou, C. Zhang, N. Chen, Int. J. Hydrogen Energy 34 (2009) 6407–6414.
[9] X. Li, H. Zhao, W. Zhou, N. Xu, Z. Xie, N. Chen, Int. J. Hydrogen Energy 35 (2010) 7913–7918.
[10] K.B. Yoo, G.M. Choi, Solid State Ionics 180 (2009) 867–871.

[11] R. Mukundan, E.L. Brosha, F.H. Garzon, Electrochem. Solid-State Lett. 7 (2004).
[12] M.R. Pillai, I. Kimb, D.M. Bierschenka, S.A. Barnett, J. Power Sources 185 (2008) 1086–1093.
[13] O.A. Marina, N.L. Canfield, J.W. Stevenson, Solid State Ionics 149 (2002) 21–28.
[14] X.Q. Fu, F. Tietz, Fuel Cells 5 (2008) 283–293.
[15] C.D. Savaniu, J.T.S. Irvine, ECS Trans. 25 (2009) 2213–2222.
[16] A. Heel, P. Holtappels, T. Graule, J. Power Sources 195 (2010) 6709–6718.
[17] O. Yamamoto, R. Takeda, R. Kanno, N. Noda, Solid State Ionics 22 (1987) 241–246.
[18] M. Sase, D. Ueno, K. Yashino, A. Kamai, T. Kawada, J. Mizusaki, J. Phys. Chem. Solids 66 (2003) 343–348.
[19] Y.J. Leng, S.H. Chan, K.A. Khor, S.P. Jiang, J. Appl. Electrochem. 34 (2004) 409–415.
[20] H. Yokokawa, N. Sakai, T. Kawada, M. Dokiya, Solid State Ionics 52 (1992) 43–56.
[21] A. Mitterdorfer, L.J. Gauckler, Solid State Ionics 11 (1998) 186–218.
[22] H.L. Tuller, Solid State Ionics 94 (1997) 63–74.
[23] A. Fujimori, J. Phys. Chem. Solids 53 (1992) 1595–1602.
[24] R. Moos, S. Schöllhammer, K.H. Härdtl, Appl. Phys. A: Mater. Sci. Process. 65 (1997) 291–294.
[25] S. Hui, A. Petric, J. Electrochem. Soc. 149 (2002) J1–J10.
[26] Q. Ma, F. Tietz, D. Stöver, Solid State Ionics (2010), doi:10.1016/j.ssi.2010.03.027.
[27] N.G. Eror, U. Balachandran, J. Solid State Chem. 40 (1981) 85–91.
[28] M.E. Bowden, D.A. Jefferson, I.W.M. Brown, J. Solid State Chem. 117 (1995) 88–96.
[29] J. Canales-Vázquez, M.J. Smith, J.T.S. Irvine, W. Zhou, Adv. Funct. Mater. 15 (2005) 1000–1008.
[30] J.C. Ruiz-Morales, J. Canales-Vázquez, C. Savaniu, D. Marrero-López, W. Zhou, J.T.S. Irvine, Nature 439 (2006) 568–571.
[31] S. Hashimoto, L. Kindermann, F.W. Poulsen, M. Mogensen, J. Alloy Compd. 397 (2005) 245–249.
[32] T.Y. Tien, F.A. Hummel, Trans. Br. Ceram. Soc. 66 (1967) 233–245.
[33] R. Moos, T. Bischoff, W. Menesklou, K.H. Hardtl, J. Mater. Sci. 32 (1997) 4247–4252.
[34] P.R. Slater, D.P. Fagg, J.T.S. Irvine, J. Mater. Chem. (1997) 2495–2498.
[35] G. Brankovic, Z. Brankovic, M.S. Góes, C.O. Paiva-Santos, M. Cilense, J.A. Varela, E. Longod, Mater. Sci. Eng. 122 (2005) 140–144.
[36] G.E. Lascalea, D.G. Lamas, E. Djurado, E.D. Cabanillas, N.E. Walsöe de Reca, Mater. Res. Bull. 40 (2005) 2029–2038.
[37] J. Sfeir, S. Vaucherb, P. Holtappels, U. Vogt, H.-J. Schindler, J. Van Herle, E. Suvorova, P. Buffat, D. Perret, N. Xanthopoulos, O. Bucheli, J. Eur. Ceram. Soc. 25 (2005) 1991–1995.
[38] P. Holtappels, U. Vogt, H. Schindler, B. Gut, in: J. Huijsmans (Ed.), Perovskite Synthesis by Spray Pyrolysis, European Fuel Cell Forum, Luzern, 2002, pp. 103–107.
[39] D. Burnat, A. Heel, L. Holzer, D. Kata, T. Graule, in: F. Krok (Ed.), Book of Poster Abstracts/Solid State Ionics, Oficyna Wydawnicza Politechniki Warszawskiej, Warsaw, 2011, p. 90.
[40] P. Blennow, K.K. Hansen, L.R. Wallenberg, M. Mogensen, Electrochim. Acta 52 (2006) 1651–1661.
[41] S.G. Cho, P.F. Johnson, J. Mater. Sci. 29 (1994) 4866–4874.
[42] G.J. McCarthy, W.B. White, R. Roy, J. Am. Ceram. Soc. 52 (1969) 463–467.
[43] M. Drys, W. Trzebiatowski, Rocz. Chem. 31 (1957) 489–496.
[44] A. Cocco, F. Massazza, Ann. Chim. 53 (1963) 982.
[45] G.L. Messing, S.C. Zhang, G.V. Jayanthi, J. Am. Ceram. Soc. 76 (1993) 2707–2726.
[46] M. Eslamian, M. Ahmed, N. Ashgriz, Nanotechnology 17 (2006) 1674–1685.
[47] K. Okuyama, I.W. Lenggoro, Chem. Eng. Sci. 58 (2003) 537–547.
[48] A. Heel, P. Holtappels, P. Hug, T. Graule, Fuel Cells 10 (2010) 419–432.
[49] A. Heel, A. Vital, P. Holtappels, T. Graule, J. Electroceram. 22 (2009) 40–46.
[50] J.H. Lee, K.Y. Jung, S.B. Park, J. Mater. Sci. 34 (1999) 4089–4093.
[51] D. Ji, W. Wend, Z. Wang, H. Zhang, P. Du, G. Shen, G. Ha, J. Electroceram. 21 (2008) 702–705.
[52] D.W. Sprosona, G.L. Messing, Commun. Am. Ceram. Soc. (1984) C92–C93.
[53] Y.C. Kang, H.S. Roh, S.B. Park, Adv. Funct. Mater. 12 (2000) 451–453.
[54] R.D. Shannon, Acta Crystallogr. A32 (1976) 751–767.
[55] S. Hashimoto, L. Kindermann, P. Larsen, F. Poulsen, M. Mogensen, J. Electroceram. 16 (2006) 103–107.